This is a “preproof” accepted article for *Quantitative Plant Biology*.
This version may be subject to change during the production process.
10.1017/qpb.2025.10013

Plant nutation relies on steady propagation of spatially asymmetric growth pattern

Mathieu Rivière[1,2], Alexis Peaucelle[1,3], Julien Derr[1,4,*], and Stéphane Douady[1]

[1]Université Paris Cité,CNRS, Laboratoire Matière et Systèmes Complexes, F-75013 Paris, France
[2]Aix Marseille Université, CNRS, IUSTI, Marseille, France
[3]Université Paris-Saclay, INRAE, AgroParisTech, Institut Jean-Pierre Bourgin, 78000, Versailles, France.
[4]Univ Lyon, ENS de Lyon, CNRS, INRAE, Inria, Laboratoire de Reproduction et Développement des Plantes, F-69007, Lyon, France
[*]To whom correspondence should be addressed. Email: julien.derr@ens-lyon.fr

Nutation is one of the most striking and ubiquitous example of the rhythmic nature of plant development. Although the consensus is that this wide oscillatory motion is driven by growth, its internal mechanisms remain to be fully elucidated. In this work, we study the specific case of nutation in compound leaves of the *Averrhoa carambola* plant. We quantify the macroscopic growth kinematics with time lapse imaging, image analysis and modeling. Our results highlight a distinct spatial region along the rachis—situated between the growth and mature zones—where the differential growth driving nutation is localized. This region coincides with the basal edge of the growth zone, where the average growth rate drops. We further show that this specific spatiotemporal growth pattern implies localized contraction events within the plant tissue.

Introduction

Plants move. This overlooked truth has come to light again thanks to the recent study of spectacular ultra-fast motions (Forterre et al., 2016). For example, the snapping of the Venus flytrap (Forterre et al., 2005; Sachse et al., 2020) and the catapulting of fern spores (Noblin et al., 2012) both require high speed cameras to be recorded. At the opposite side of the timescales spectrum, plants moves through their growth.

The observation of these slow motions necessitate time-lapse imaging. After Darwin (Darwin, 1897), they started to be historically investigated with the development of photography (Gaycken, 2012). But we are still evidencing nowadays a variety of exciting new motions (Riviere et al.` , 2017, 2020; Derr et al., 2018). They can either be nastic motions, or tropisms, depending on whether the direction of the motion is imposed by factors internal or external to the plant respectively. The movement is defined as autonomic (respectively paratonic) depending on whether the triggering signal is internal to the plant or not. They can finally be reversible or linked to irreversible growth. These three dichotomies define the traditional classification of slow plant motions (Riviere` et al., 2017). Within this framework, the status of one remarkable movement called nutation is still undecided (Rivière et al. , 2017; Stolarz, 2009; Baskin, 2015; Mugnai et al., 2015)

Nutation is the phenomenon that causes the orientation of the long axis of an elongated growing plant to vary over time in a pseudo-periodical way. It was already observed for climbing plants by British botanists of the 17th century (Webster, 1966) and began to be studied by Hugo von Mohl and Ludwig Palm in the first part of the 19th century (Baillaud, 1957). To the best of our knowledge, the term ”nutation” was first mentioned by Charles Bonnet (Bonnet, 1754) although he acknowledges that this term had been named before him, by physicists who knew the phenomenon. They probably saw this motion as a botanical analog to the astronomical nutation.

Darwin later introduced the idea that nutation had an endogenous origin and many plant motions were actually modified nutations (Darwin, 1897). The very origin of nutation was a source of debate at the time nonetheless (Baillaud, 1957), and it remains so up to this date (Brown, 1993; Migliaccio et al., 2013; Mugnai et al., 2015). Part of the community backs up Darwin’s idea of an internal oscillator (Brown et al., 1990; Johnsson et al., 1999). Others ascribe this oscillating behaviour to inertial overshooting of the plant occurring during its straightening process (Israelsson and Johnsson, 1967; Johnsson and Israelsson, 1968; Gradmann, 1922; Agostinelli et al., 2020). Finally, the compromise solution calling for a combination of these two hypotheses gathers more and more support (Johnsson et al., 1999; Johnsson, 1997; Orbovic and Poff´ , 1997; Stolarz, 2009; Agostinelli et al., 2021). The one thing making consensus is that nutation is a macroscopic manifestation of multicellular microscopic growth.

Plant growth results from a subtle balance between the strong internal osmotic pressure and the resisting rheology of the cell wall (Tomos et al., 1989). Although growth and plasticity are very distinct processes, and growth doesn’t involve viscosity (Goriely, 2017), Lockhart used an effective viscoplastic framework to formalize plant growth (Lockhart, 1965). Lockhart’s model received good experimental support at the single cell level (Green et al., 1971; Cosgrove, 1985; Zhu and Boyer, 1992). Still, some shortcomings need to be addressed (Jordan and Dumais, 2010), and the origin of the cell wall-loosening mechanism remains unclear (Palin and Geitmann, 2012; Kroeger et al., 2011; Micheli, 2001; Höfte et al., 2012). The cell wall is considered here to be an inactive gel but it was demonstrated that elements of the cell wall, the homogalacturonans (HG) can transform chemical modification into mechanical expansion through cell controlled enzymatic demethylesterification (Haas et al., 2020). The precise role of elasticity that was added to Lockhart model later on by Ortega (Ortega, 1985) is then subject to debate (Kierzkowski et al., 2012; Haas et al., 2020). Finally, The multi-cellular aspect of the biophysics of growth remains to be understood (Boudon et al., 2015). In particular, dynamical aspects related to water fluxes between cells have just started to be taken into account, either numerically (Cheddadi et al., 2019) or even more recently theoretically with the development of a hydromechanical field theory for plant morphogenesis (Oliveri and Cheddadi, 2025). These new theoretical concepts will be key to understand the complex spatio-temporal behaviour observed in plant nutations.

The seminal work on the spatio-temporal characterization of nutation has been performed by Berg and Peacock (Berg and Peacock, 1992) where they evidenced strong fluctuations and traveling waves of the axial elongation rate in the sunflower hypocotyl. They even measured negative rates, suggesting local contractions. At the time, they acquired data with one single camera, and their growth measurements were necessarily biased by strong projection artifacts due to the three-dimensional nature of the motion.

Here, we aim to revisit in detail the phenomenon of nutation. By carefully quantifying the motion of nutation (taking into account the 3D nature of the motion), we will gain knowledge on the nature of this puzzling mechanism. In this article, we focus on the plant *Averrhoa carambola*, a plant known for exhibiting ample nutation (see Fig. 1A–B) and other growth motions (Rivière et al. , 2017, 2020; Rivière , 2017).

The manuscript is organized as follows. We start by characterizing the kinematics of nutation at the scale of the whole leaf, and emphasize the spatial organization of growth. Our measurements allow to characterize the growth law of nutation and highlight a relationship between mean growth and differential growth. We then zoom in on the bending zone and, thanks to a kinematics model, analyze contraction events. Finally, we put our results in perspective with the microscopic properties (elasticity and chemical content) of the plant cell wall.

Materials and methods

Growth conditions of plants

Averrhoa carambola seeds were directly obtained from commercially available fruits and sown into all-purpose compost. Young seedlings were first kept inside a small lab greenhouse. Older plants (> 6 months) were then moved to the experimentation room. There, plants were submitted to a 12/12 light cycle under ORTICA 200W 2700K culture lamps. The temperature and relative humidity rate were monitored with a DHT22 sensor. Temperature was usually comprised between 20 ^oC and 24 ^oC. The relative humidity rate was around 60%. All methods were performed in accordance with the relevant guidelines and regulations.

Kinematics: sample preparation

The rachis of interest was carefully coated with fluorescent pigments with a brush. For curvature and coarse elongation measurements, the top of the rachis was coated homogeneously with orange pigments. Small blue fluorescent dots were added to mark the nodes and the petiole. For fine measurements of local growth, the orange pigments were deposited on the face of a few interfoliolar segments so that they form highly textured and contrasted patterns. In both cases, because of growth, pigments needed to be added manually on a regular basis to compensate the dilution of the signal over time.

Kinematics: image acquisition

The kinematics of nutation were captured using time-lapse photography with a DSLR camera controlled with the open-source software gPhoto2. The camera was firmly fixed to a rigid structure to avoid any displacement or rotation. The built-in flash of the camera was covered with LEE Moss green filter and set to the lowest intensity to keep light input minimal during nights. For curvature and coarse growth kinematics, top-views were taken every 2.5 min. For local growth measurements, side-views were taken every minute.

Kinematics: data analysis

The midline, or skeleton, of the rachis was obtained by first thresholding the red channel of the pictures. A cloud of points was obtained and then reduced to a smooth line with a moving median filter. The curvature of the rachis $\kappa_\perp$ in the plane of interest was obtained by locally fitting the midline to a circle. The position of the leaflets was retrieved by thresholding the blue channel. Because of growth, blues dots dilated, lost intensity in time and sometimes even split. The global unfurling motion of the rachis sometimes resulted in a temporary occlusion of some blue dots. Simple rules on the conservation of these dots, distance between consecutive dots and displacements values could overcome a majority of tracking failures. Manual correction was still needed in some special cases. Finally, the presented spatiotemporal graphs were smoothed with 2D averaging and median filters.

Kinematics: fine measurements

We obtain the skeleton of the rachis by a simple geometric transformation of the upper contour which is less altered by leaflet motions. Then we measure the the elongation field along the rachis by using a previously published image-to-image correlation (Bastien et al., 2016). The time-frequency analysis of the elongation signals was done by using MATLAB's continuous wavelet transform toolbox. We used the 'cgau2' mother wavelet (second order derivative of the complex Gaussian). For each location of the rachis, $\dot{\varepsilon}(t)$ was wavelet-transformed. From the resulting complex coefficients $C_{a,b}$ we extracted information on the weight of each scale/frequency in the signal by computing an 'energy':$E(a) = \sum_b \left|C_{a,b}\right|^2 / \sum_a \sum_b \left|C_{a,b}\right|^2$, where a and b are the scale and shift parameters of the wavelet transform. This information was then re-aggregated and re-arranged to build kymographs displaying the weight of frequencies in the elongation signal along the rachis.

Kinematic model of nutation

The rachis is modelled by a two-dimensional beam of width $2R$ (see Fig. S1) and of total length L_{tot}. The geometry of the midline is then described with the same quantities than the actual leaf (see Fig. 1C). The model contains only a few essential ingredients:

1. We define the *elongation rate* ˙ as the relative local growth rate of an element. For example, at arclength s, an element of size δs as the following local relative growth rate:

$$\dot{\varepsilon}(s) = \frac{1}{\delta s}\frac{d\delta s}{dt} \quad (1)$$

   The lateral faces of the beam can have different elongation rates $\dot{\varepsilon_L}$ and $\dot{\varepsilon_R}$, giving rise to differential elongation $\dot{\delta}$. We assume that the profile of elongation is linear in the bulk of the rachis:

$$\begin{cases} \dot{\varepsilon} = (\dot{\varepsilon_R} + \dot{\varepsilon_L})/2 \\ \dot{\delta} = (\dot{\varepsilon_R} - \dot{\varepsilon_L})/2 \end{cases} \quad (2)$$

2. An apical growth zone of length L_{gz} of constant length. The elongation rate of the midline $\dot{\varepsilon}$ is thus independent of time and given by:

$$\dot{\varepsilon}(s_a) = \frac{\dot{\varepsilon}_0}{2}\left(1 - \tanh\left(\frac{s_a - L_{gz}}{\Delta L}\right)\right) \quad (3)$$

   where s_a is the arc length starting from the apex, and ΔL the typical length scale of variation of $\dot{\varepsilon}$.

3. Differential elongation occurs where the mean elongation rate drops, within a bending zone of length $2\Delta L$ (for justification, see Results). Because nutation is a periodical oscillatory motion, differential elongation is modulated by a sine of frequency $2\pi/\omega$:

$$\dot{\delta}(s_a, t) = \dot{\delta}_0 \left(1 - \tanh^2\left(\frac{s_a - L_{gz}}{\Delta L}\right)\right) \tag{4}$$

4. We assume differential elongation is the unique driver of the bending of the rachis. In our case, since the period of nutation is much smaller than the typical time scale of elongation, we furthermore neglect the advection of curvature. In this case, differential elongation rates ($\dot{\delta}$) and the rate of change of curvature ($d\kappa/dt$) have been shown to be equivalent (Silk, 1984; Jensen and Forterre, 2022). Their relationship is purely geometric and can be simplified in the case $R\kappa_\perp \ll 1$ (for us, $R\kappa_\perp \sim 10^{-2}$). We follow the kinematic calculation provided by Bastien (equation A.43 in (Bastien, 2010)) with second order correction in $R\kappa_\perp$ to write:

   $$\frac{\partial \kappa_\perp}{\partial t} \approx \frac{1 - R^2\kappa^2}{R}\,\dot{\delta} \text{ (5)}$$

   Interestingly, equation 5 does not display the dilution of curvature due to average growth. Chavarria showed that the dilution effect is compensated by curvature creation (Chavarr´ıa-Krauser, 2006).

The model was implemented numerically with discretized versions of the kinematic equations 3, 4 and 5. When and where $\dot{\varepsilon} < |\dot{\delta}|$, local contractions will occur along the lateral faces of the rachis–ie. either $\dot{\varepsilon}_R < 0$ or $\dot{\varepsilon}_L < 0$ over a finite spatial extent (see Fig. S1). This depends on the relative values of $\dot{\delta}_0$ and $\dot{\varepsilon}_0$ and the exact threshold depends on the spatial functions chosen to describe $\dot{\varepsilon}$ and $\dot{\delta}$. Here, a sufficient condition for contractions is $\dot{\varepsilon}_0 \leq \dot{\varepsilon}_c = 4\dot{\delta}_0$. Finally, the apparent elongation $\dot{\varepsilon}_\perp$ observed by a camera is obtained by measuring the orthogonal projection of the simulated rachis onto the plane of observation (see Fig. S2).

Results

Characterizing nutation

As they grow, *Avherroa carambola* compound leaves exhibit pronounced growth motions. Putting aside the leaflets, the motion of the rachis can be broken down into two different motions, depending on their plane of occurrence (for anatomical terms, see Fig. S3). The unfurling motion of the rachis of *Avherroa carambola* mostly takes place

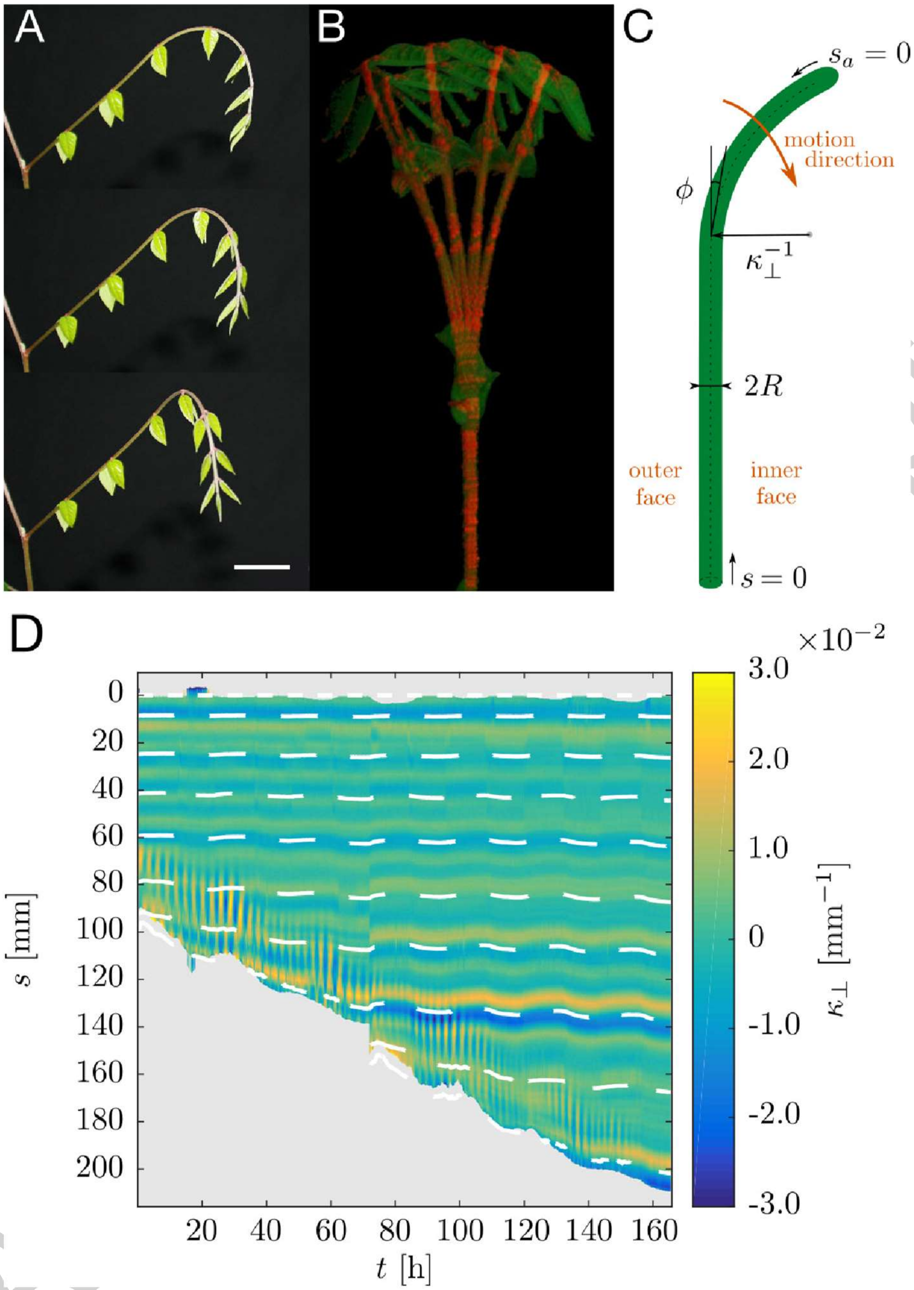

Figure 1: **Nutation movement of an *Averrhoa carambola* compound leaf. (A)** Side view, 30 minutes between pictures from top to bottom. The hook shape gradually comes out of the plane towards the observer **(B)** Top view, 15 min between pictures (nutation period usually varies between 1.5 and 4 hours). The distal end of the leaf oscillates in a pendulum-like fashion, orthogonal to the rachis' axis. After a full period, the leaf has elongated. **(C)** Geometrical parameters describing the rachis and nutation: arclengths s and s_a (from the base or the apex respectively), local angle φ, local curvature $\kappa_\perp$ and radius R. The direction of motion defines the

outer and inner faces of the rachis. **(D)** Spatiotemporal diagram of the curvature7 $\kappa_\perp(s, t)$ along the rachis obtained from a top-view time lapse movie. Oscillations of $\kappa_\perp(s, t)$ are visible close to the apex.
Dashed white lines mark the position of leaflets.

in a principal plane (Rivière et al. , 2017). The rachis unfolds steadily while propagating a hook shape (Rivière et al., 2020). This hook shape is visible in Fig. 1A. This motion is also accompanied by out-of-plane curvature variations. The rachis bends and unbends in a pseudo-periodical way, as if it were oscillating around a rectilinear state. The oscillations can already be seen in Fig. 1A. In Fig. 1B, we see the same motion from the top and on a slightly longer time range. The period of oscillation varies greatly between 1.5 and 4 hours, typically between 2 and 3 hours, while the typical amplitude is of the order of 25 degrees. **Supporting movie 1** shows a time-lapse movie of a typical nutation motion, seen from both sides. To properly describe the nutation motion, we define: the base-to-apex arc length s, and s_a its apex-to-base counterpart ; φ the local angle with respect to the average direction of the rachis ; and the curvature $\kappa_\perp$ (see Fig. 1C). Fig. 1D shows the quantification of $\kappa_\perp$ in both time and space.

Elongation and bending are localized

We measured the average elongation rate $\dot{E}$ of each of the successive interfoliolar segments by tracking the position of the successive nodes. The spatiotemporal diagram of $\dot{E}$ shows that only the apical-most region of the rachis elongates, defining a growth zone near the apex (see Fig. 2A).

We then estimated the profile of differential elongation $\dot{\delta}$ along the rachis from the transverse curvature $\kappa_\perp$ measurement, thanks to the several hypotheses described in the Material and Methods section. Its envelope was estimated via a method based on the Hilbert transform (Kincaid, 1966) (for more details, see supplementary text). The evolution in time and space of the envelope of $\dot{\delta}$ is displayed in Fig. 2B. We see that the differential growth—hence the bending—is spatially limited to a zone downstream of the apex. Similarly to what is done for the elongation, it is thus possible to define a bending zone.

This bending zone is at a roughly constant distance from the apex, similarly to the constant length of elongation zone from the apex (see Fig. 2B). Finally, going a step further in the description of nutation, we notice that the amplitude of the differential elongation—or of the bending—varies in time, reaching a maximum of 3×10^{-2} h^{-1}. These slow amplitude modulations of nutation are, however, not in the scope of the present study.

Differential elongation peaks where elongation drops

Because the growth spatial profile is almost steady in the frame of reference of the apex, we can average the measured quantities in time. The averaged quantities $\dot{E}$ and $\dot{D}$ corresponding to mean elongation and differential elongation rates of interfoliolar segments are plotted on Fig. 3. Both profiles confirm the existence of a localized

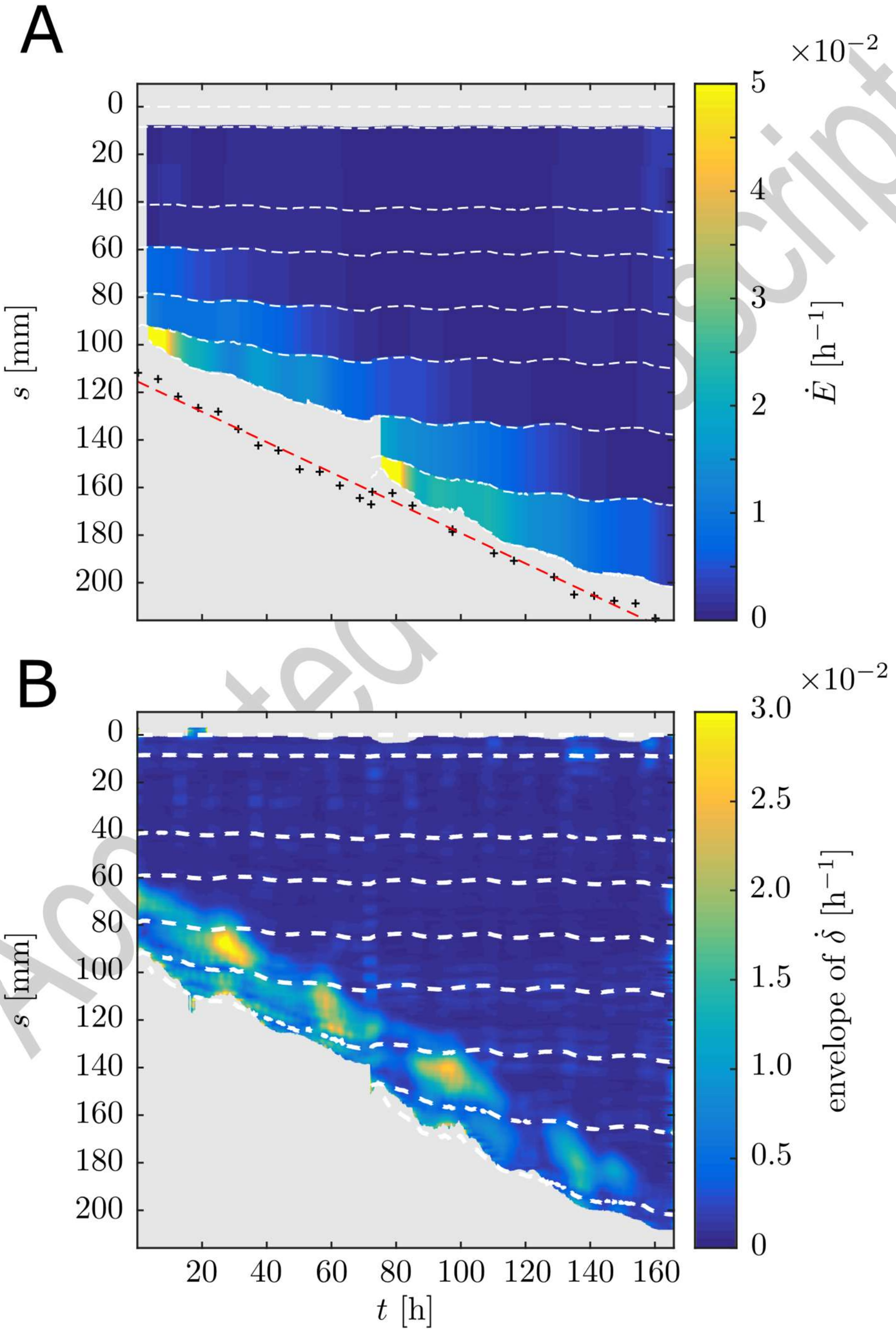

Figure 2: **Elongation and estimated differential elongation during nutation. (A)** Spatiotemporal diagram of the elongation rate $\dot{E}$ of each interfoliolar segment estimated from the leaflets' trajectories (white dotted lines). The black crosses show the position of the leaf apex estimated from side-view pictures. The red dashed line is a linear fit of the apex position. **(B)** Spatiotemporal diagram of the envelope of differential elongation $\dot{\delta}$ estimated from the curvature diagram (nutation amplitude).

growth zone. The typical length scale is about 50 mm, and beyond 100 mm growth is not detectable at all. The mean elongation rate looks like a sigmoid function. In the growth zone the typical elongation rate is of the order of 10^{-2} h^{-1}, consistently to typical averaged values found in the literature (Poorter and Remkes, 1990; Lambers and Poorter, 1992), and then decays to zero. Interestingly, the differential elongation rate behaves differently. It is non-monotonic and its maximum coincides with the edge of the growing zone, where the mean elongation rate drops. A simple mathematical description of these sigmoid and peaked shapes is well fitted with the hyperbolic functions similar to Eq. 3 and 4. The results are displayed Fig. 3. In this case the derivative of the fit of the longitudinal elongation rate matches well our experimental measurements of the differential elongation rate, with its amplitude remaining a free parameter (see supplementary text).

The elongation profile in the growth zone is compatible with local contractions

We used techniques inspired from digital image correlation (see Materials and Methods) to quantify the elongation profile within the bending zone. However, as the nutation moves the rachis towards or away from the camera, we can only measure an *apparent* elongation rate (see Fig. S4 and associated supplementary text). Strong projection artifacts indeed affect our measurements: we see oscillations and even negative values of $\dot{\varepsilon}_{\perp}$ (see Fig. 4A).

Strikingly, the period of oscillation depends on position (see Fig. 4A). Oscillations are faster at the apical end of the sample (top on graph), and slower at its basal end (bottom on graph). A wavelet transform evidences two distinct dominant modes with periods in a 2:1 ratio (see Fig. 4B). We measured $\tau_f \approx 2.1$ h at the basal end— corresponding to the nutation period—and $\tau_{2f} \approx 1.2$ h at the apical end. In an attempt to rationalize these artifacts, and to work around them, we built a simple model based on the experimental kinematic features of nutation and also accounting for projection effects (see Materials and Methods). This model first provides an order of magnitude for differential growth. Indeed, it can be shown that:

$$\Delta\phi = 2\Delta L \frac{\dot{\delta}_0}{R\omega} \quad (6)$$

This can be understood as $\dot{\delta}_0/\omega$ being the total differential growth over one period of nutation, which divided by the radius R gives the local curvature of the rachis, and integrated over the bending zone length $2\Delta L$, gives the final deviation of the apex (see supplementary text for formal derivation). By injecting estimations in this relationship ($\Delta\phi \sim \pi/6$, $2\pi/\omega \sim 2$ h, $R \sim 0.25$ mm and $\Delta L \sim 50$ mm), we find $\dot{\delta_0} \sim 7.5 \times 10^{-3}\text{h}^{-1} \sim 10^{-2}\, h^{-1}$ matching the order of magnitude of the measured averaged growth, thus

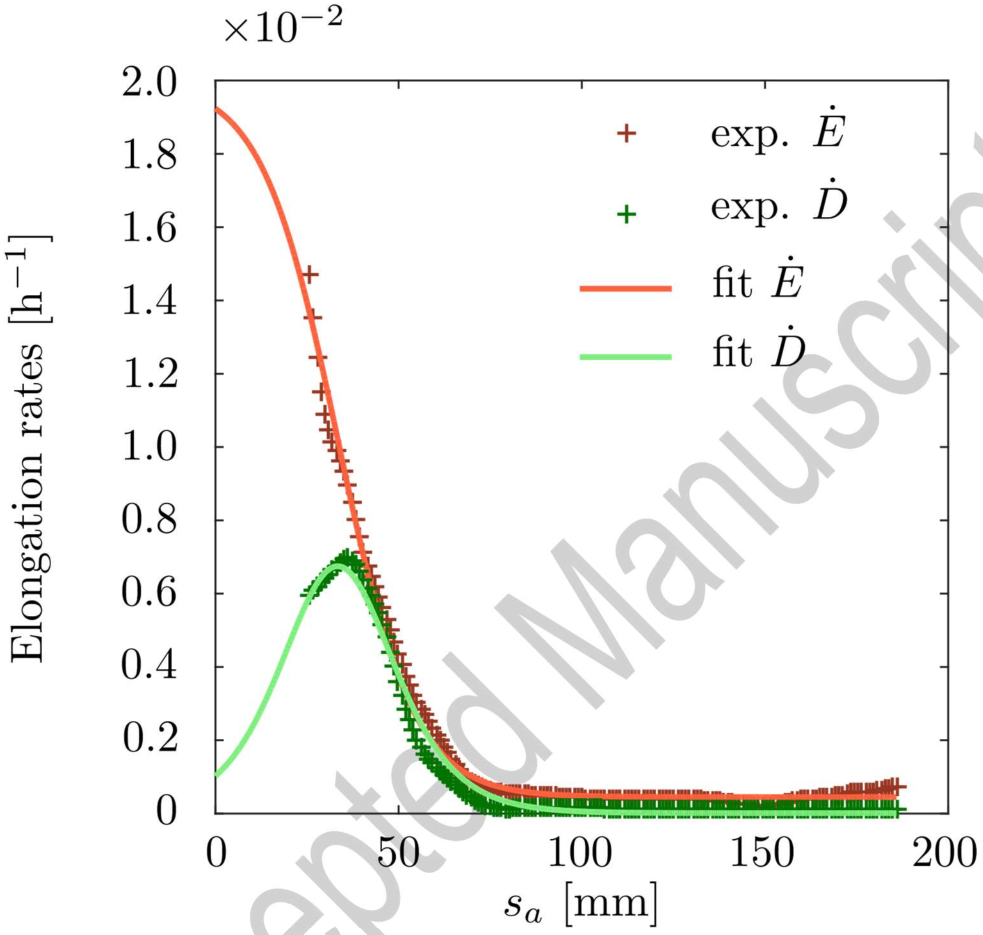

Figure 3: **Average spatial profiles of elongation rate and differential elongation rate**. The two profiles were fitted respectively to a sigmoid (red line) and to its derivative (green line). The complete profiles cannot be measured from a top-view because of the hook shape of the leaf.

confirming the possibility of contractions.

Second, simulations our model reproduce the observed pattern of $\dot{\varepsilon}_\perp$ (see Fig. 4C– D). Our model indeed shows that the two main oscillating contributions to $\dot{\varepsilon}_\perp$ are brought by: (i) projection (geometrical) effects, with frequency double that of nutation, maximum at the apical end of the rachis ; and (ii) the differential elongation itself, with frequency equal to that of nutation, peaking around $s_a = L_{gz}$ (see supplementary text for more details). While oscillations of $\dot{\varepsilon}_\perp$ at τ_{2f} are expected in any case (see Fig. S4), oscillations with period τ_f are a direct signature of differential elongation.

Finally, we fit the wavelet transform spatiotemporal diagram as a way to estimate the unknown experimental parameters. The best fit is presented in Fig. 4C and D. The corresponding parameters $\dot{\delta}_0 = 4.5 \times 10^{-3}\,\mathrm{h}^{-1}$ and $\dot{\varepsilon}_0 = 1.4 \times 10^{-2}\mathrm{h}^{-1}$ indicate that the rachis *must* locally contract to explain our experimental measurements.

Discussion

The nutation zone is spatially linked to the growing zone and undergoes "stop and go" phenomena

The kinematics of nutation presented here are consistent with our previous study on the same system and confirm the presence of a steady growth zone, extending from the apex over a constant length (Rivière et al., 2020). This is also in agreement with growth spatial profiles observed in roots (Silk et al., 1989; Walter et al., 2002; Chavarría-Krauser et al., 2008; Quiros et al., 2022), and several cylindrical aerial organs (Silk, 1992; Peters and Tomos, 2000; Bastien et al., 2018).

We also show that the basal end of the growth zone coincides with the nutation zone — ie.fluctuations of the differential elongation rate . The spatial coincidence of the maximum of the differential elongation rate with the region of steepest decrease of the average elongation rate is consistent with previous observations on *Arabidopsis thaliana* roots (Chavarría-Krauser et al., 2008). This phenomenon could be compatible with the existence of a maximum value for the elongation rate, likely set by a combination of environmental factors and inner physiological constraints. Close to the apex, growth-regulating signals could be so strong that the elongation saturates by far. Small perturbations of these signals in space or time would not affect the saturated elongation rate and would get edged out. Conversely, when and where they are not strong enough to saturate elongation anymore, any perturbation on the growth-regulating signals could directly affect the elongation rate and would eventually translate into oscillations. The basal end of the growth zone would then be the location most prone to such variations. The same interpretation could apply to oscillations during the gravit-

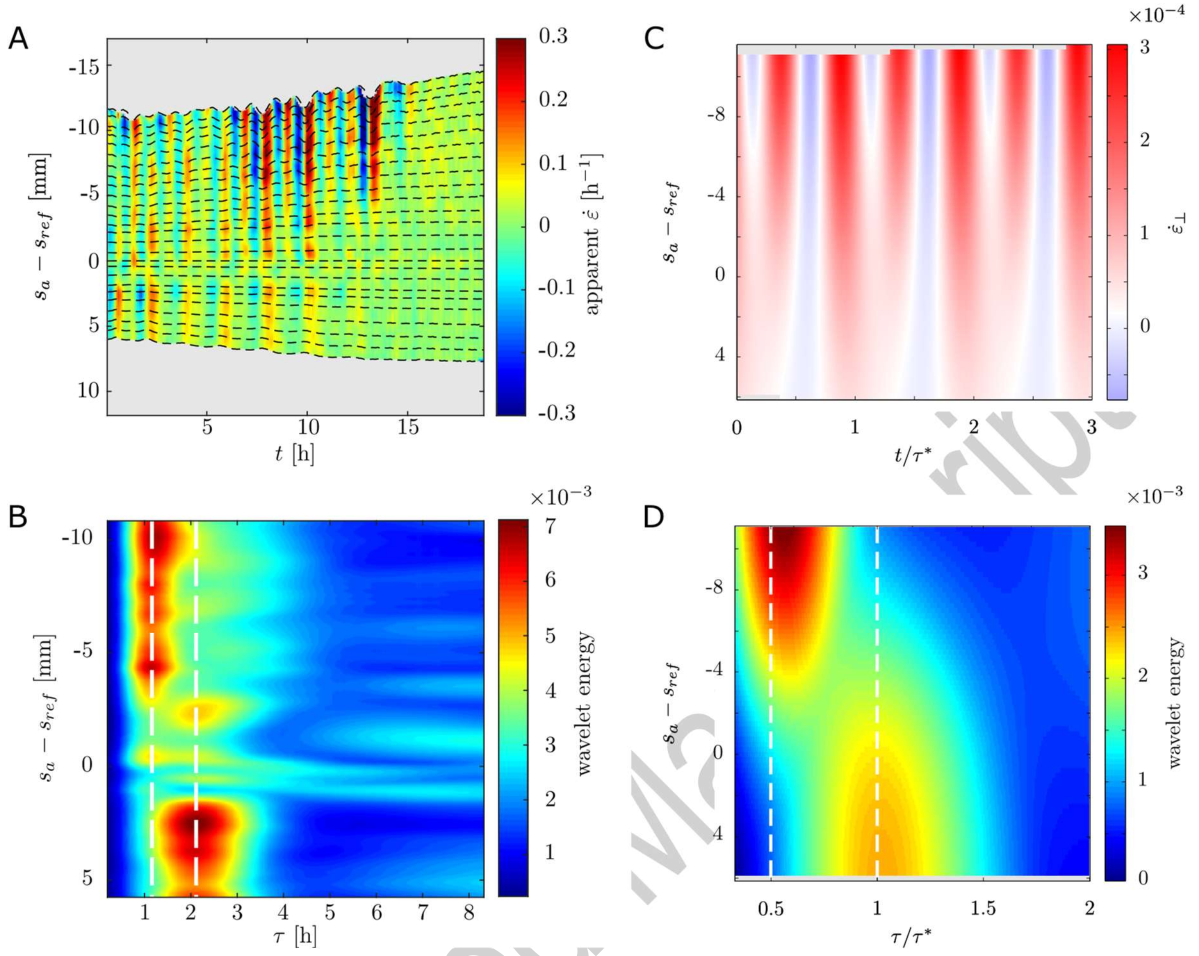

Figure 4: **(A)** Spatiotemporal diagram showing an experimental measurement of the *apparent* local elongation rate $\dot{\varepsilon}$ in the bending zone from a side-view time lapse movie. Because of the oscillatory motion of the rachis, the elongation rate measured is affected by projection effects. **(B)** Wavelet decomposition of the experimental spatiotemporal diagram of apparent elongation rate. The decomposition shows that two dominant modes in the signal: $\tau_{2f} \approx 1.2$ h and $\tau_f \approx 2.1$ h respectively close to the apical and basal ends of the observed section of the rachis. **(C)** and **(D)**: Best fit of the kinematics model to the experimental data; $\Delta\phi = 8^\circ$, $L_{gz} = 20.6$ mm, $\Delta L = 12.2$mm, $\dot{\delta}_0 = 4.5 \times 10^{-3}\,\mathrm{h}^{-1}$ ($\dot{\varepsilon}_0 = 1.4 \times 10^{-2}\,\mathrm{h}^{-1}$, $R = 0.26$mm were measured and fixed before fitting). This set of parameters allows local contractions.

ropic straightening of wheat coleoptiles (Bastien et al., 2018): as the coleoptile bends towards the vertical, the differential growth signal is at its maximum, and no oscillation is observed. On the contrary, when the coleoptile approaches a vertical posture, the signal decreases, and nutation of the tip becomes visible again.

Quantitatively, when and where the differential elongation rate is maximum, its amplitude is also comparable to the local average elongation rate (see Fig. 3) making the total growth of one side close to zero or even possibly negative. This could be schematized as a “stop and go” phenomenon, where each side of the rachis grows alternately, before growth and motions cease altogether. This alternate growth behavior was already apparent in pea’s epicotyls observation(Baskin, 1986).

Contraction events during plant growth

In all generality, the spatial arrangement of the average elongation rate $\dot{\varepsilon}$ and the differential elongation rate $\dot{\delta}$ can lead to local contractions within the bending zone depending on their relative amplitudes (see Fig. 3D). Our local measurements of $\dot{\varepsilon}$ in the bending zone (see Fig. 4A–B), interpreted by taking projection effects into account, indirectly revealed that nutation in *Averrhoa carambola* rachis is compatible with local contraction events—ie. negative elongation rates over finite spatial extent—(see Fig. 4). These results are in line with previous reports of contraction events in the circumnutating stems of several other species (Baskin, 1986; Berg and Peacock, 1992; Caré et al. , 1998; Stolarz et al., 2008), both at the cell and tissue levels. It was also observed that contractions are circumscribed to either the basal end of the growth zone—where the average elongation rate decays— (Berg and Peacock, 1992), or to the bending zone (Caré et al., 1998), consistently with our findings.

Reports of contractions and negative growth rates go beyond the sole context of nutation. They have indeed been observed during shoot apical meristem morphogenesis (Kwiatkowska and Dumais, 2003; Kwiatkowska, 2006; Kwiatkowska and Routier-Kierzkowska, 2009; Long et al., 2020) and simple leaf growth (Armon et al., 2021), both at the cellular and organ scales.

The interpretation of negative growth rates is still a matter of debate in the community. In 1992, Berg and Peacock, attributed tissue contractions to a purely elastic behaviour (Berg and Peacock, 1992). In 1998, Care *et al.* showed that tissue contractions were not artifacts but instead due to local cell contraction driven by osmotic changes (Caré et al. , 1998). Only recently, theories describing both elasticity and osmotic water fluxes between cells in plants (Cheddadi et al., 2019; Oliveri and Cheddadi, 2025) have shown that water motion effects are central in plant morphogenesis: a growing tissue acts as a sink and extract water from neighbouring cells which acts like source. In our case, during the nutation movement, the growing side could get water from the opposite side, leading to contractions of the latter.

A window on the physiological implications of nutation and growth

We believe that growth motions, and nutation in particular, offer an experimental framework to probe growth at the microscopic scales. Its oscillatory nature combined with a clear spatial pattern allow to probe a variety of cell-wall mechanics, cell-wall chemical status and macroscopic growth rates combinations. A full microscopic investigation goes beyond the scope of this paper but we provide in supplemental material, a set of preliminary experiments constituting a proof of concept.

First possible experiment is to use our nutating system to probe cell wall elasticity in growing or not growing tissue. Our preliminary experiments seem to indicate a strong correlation between elasticity and growth: the growing side is found softer than the nongrowing side (see Fig. S4, and corresponding text). This belongs to a long series of observations correlating growth with changes in cell wall elasticity, by suggesting that growth is faster where the Young's modulus is lower. This phenomenon was evidenced in growing pollen tips (Zerzour et al., 2009), maize roots elongation zone (Abeysekera and McCully, 1994; Kozlova et al., 2019), *Arabidopsis* shoot meristem before primordia formation (Milani et al., 2011; Peaucelle et al., 2011). Similarly, we can probe the changes in chemical status during growth, and our preliminary experiments seem to indicate a change in methylesterification status of the pectins if the tissue is growing or not (see Fig. S5 and associated text).

In our system it is difficult to disentangle the reversible and irreversible contributions to growth as it was done by Proseus *et al.* for the single-cell algae *Chara* (Proseus et al., 1999). It has also been shown in the case of the shoot apical meristem that elastic inhomogeneities (or differences in stress stiffening) could lead to differential growth (Kierzkowski et al., 2012). Therefore, to discuss the missing link between the observed microscopic properties and the macroscopic contractions, we propose two different hypothetic scenarios.

First, one should consider the reversible processes as they have already been found to be involved in nutation and growth. As mentioned before, Cheddadi *et al.* recently formalized the water fluxes coupling in multicellular organs. They showed in particular that new types of lateral inhibitory mechanisms could amplify growth heterogeneities (Cheddadi et al., 2019): Tthe softer tissues are favored to become sinks for water at the expense of the neighbouring cells. In order to investigate this scenario further, one will need to extend the model to incorporate mechanical aspects. Recently, Moulton *et al.* generalized the analytical results of Timoshenko about the growth of 2D bimetallic strips(Timoshenko, 1925) to filaments in 3D (Moulton et al., 2020a). This new framework which already proved successful to reproduce plant tropism(Moulton et al., 2020b) is an exciting new line of investigation for nutation.

From our preliminary observations, one could also propose a second hypothetical scenario for the temporal events: on the growing side, HG are actively addressed to the cell wall in their native methylated way. Then growth turns to the other side of the rachis following an external or internal signal, and HG are sparsely degraded or recycled by endoglucanase explaining the reduction in staining observed in methylated and demethylated pectins. Here we can indicate that the time scale could be as fast as 30 minutes. Haas *et al.* (Haas et al., 2020) proposed that the expansion part could be solely due to HG filament expansion following the de-methylesterification. In addition, the partial removal of the highly charged polymer following their recycling could as well lead to cell wall compaction in link with the observed tissue contraction.

Conclusion

To sum up, we provided on a new biological model case (*Averrhoa carambola*), a complete kinematic description of the nutation motion paying especially attention to the 3D effects. Thanks to a kinematic model we could disentangle the projection artifacts, and prove that contractions really happen during nutation. Nutation is found to occur as a steady propagation spatial growth pattern showing co-localization of the peak of differential growth with the onset of the growing region. Finally, we showed that this macroscopic behavior can be used as a tool to investigate microscopic properties of the dynamically alternating growing tissues.

Acknowledgements

The authors thank Elliot Meyerowitz and Raymond Wightman for their support and help on the immunolabelling experiments. We are also grateful to Olivier Hamant and Emmanuel de Langre for continuous feedback on our works. MR is grateful to "Ecole Doctorale Frontières du Vivant - Programme Bettencourt" for financial support.

Author contributions statement

All authors designed the research. MR and JD performed kinematics experiments. MR and AP performed microscopic investigation. MR and SD designed the model. MR performed numerical simulations. MR and JD analyzed the data. All authors discussed the results. MR and JD drafted the paper. All authors edited the manuscript.

Financial support

This research received no specific grant from any funding agency, commercial or notfor-profit sectors.

Conflicts of interest

None.

Data and Coding Availability

The datasets generated during and/or analysed during the current study are available in the Zenodo repository, https://doi.org/10.5281/zenodo.7994913; **Competing interests** The authors declare no conflict of interest.

Financial support This research received no specific grant from any funding agency, commercial or not-for-profit sectors.

References

R. Abeysekera and M. McCully. The epidermal surface of the maize root tip: Iii. isolation of the surface and characterization of some of its structural and mechanical properties. *New phytologist*, 127(2):321–333, 1994.

D. Agostinelli, A. Lucantonio, G. Noselli, and A. DeSimone. Nutations in growing plant shoots: The role of elastic deformations due to gravity loading. *Journal of the Mechanics and Physics of Solids*, 136:103702, 2020.

D. Agostinelli, A. DeSimone, and G. Noselli. Nutations in plant shoots: endogenous and exogenous factors in the presence of mechanical deformations. *Frontiers in plant science*, 12:608005, 2021.

S. Armon, M. Moshe, and E. Sharon. The multiscale nature of leaf growth fields. *Communications Physics*, 4(1):1–7, 2021.

L. Baillaud. *Recherches sur les mouvements spontanés des plantes grimpantes* . Carrère, 1957.

T. Baskin. Redistribution of growth during phototropism and nutation in the pea epicotyl. *Planta*, 169(3):406–414, 1986.

T. I. Baskin. Ultradian growth oscillations in organs: physiological signal or noise? In *Rhythms in Plants*, pages 3–17. Springer, 2015.

R. Bastien. *Formes et mouvements gravitropiques des tiges vegétales: Modèle universel et phénotypage*. Thèses, Université Paris-Diderot - Paris VII, Oct. 2010. URL https://theses.hal.science/tel-00764999.

R. Bastien, D. Legland, M. Martin, L. Fregosi, A. Peaucelle, S. Douady, B. Moulia, and H. Höfte. Kymorod: a method for automated kinematic analysis of rod-shaped plant organs. *The Plant Journal*, 88(3):468–475, 2016.

R. Bastien, O. Guayasamin, S. Douady, and B. Moulia. Coupled ultradian growth and curvature oscillations during gravitropic movement in disturbed wheat coleoptiles. *PloS one*, 13(3):e0194893, 2018.

A. R. Berg and K. Peacock. Growth patterns in nutating and nonnutating sunflower (helianthus annuus) hypocotyls. *American Journal of Botany*, 79(1):77–85, 1992.

C. Bonnet. *Recherches sur l'usage des feuilles dans les plantes: et sur quelques autres sujets relatifs à l'histoire de la végétation*. chez Elie Luzac, fils, 1754.

F. Boudon, J. Chopard, O. Ali, B. Gilles, O. Hamant, A. Boudaoud, J. Traas, and C. Godin. A computational framework for 3d mechanical modeling of plant morphogenesis with cellular resolution. *PLoS Comput Biol*, 11(1):e1003950, 2015.

A. H. Brown. Circumnutations: from darwin to space flights. *Plant Physiology*, 101(2): 345, 1993.

A. H. Brown, D. K. Chapman, R. F. Lewis, and A. L. Venditti. Circumnutations of sunflower hypocotyls in satellite orbit. *Plant Physiology*, 94(1):233–238, 1990.

A.-F. Care, L. Nefed'ev, B. Bonnet, B. Millet, and P.-M. Badot. Cell elongation and revolving movement in phaseolus vulgaris l. twining shoots. *Plant and cell physiology*, 39(9):914–921, 1998.

A. Chavarría-Krauser. Quantification of curvature production in cylindrical organs, such as roots and hypocotyls. *New Phytologist*, 171(3):633–641, 2006.

A. Chavarría-Krauser, K. A. Nagel, K. Palme, U. Schurr, A. Walter, and H. Scharr. Spatio-temporal quantification of differential growth processes in root growth zones based on a novel combination of image sequence processing and refined concepts describing curvature production. *New Phytologist*, 177(3):811–821, 2008.

I. Cheddadi, M. Génard, N. Bertin, and C. Godin. Coupling water fluxes with cell wall mechanics in a multicellular model of plant development. *PLoS computational biology*, 15(6):e1007121, 2019.

D. J. Cosgrove. Cell wall yield properties of growing tissue: evaluation by in vivo stress relaxation. *Plant physiology*, 78(2):347–356, 1985.

C. Darwin. *The power of movement in plants*. Appleton, 1897.

J. Derr, R. Bastien, E. Couturier, and S. Douady. Fluttering of growing leaves as a way to reach flatness: experimental evidence on persea americana. *Journal of the Royal society interface*, 15(138):20170595, 2018.

Y. Forterre, J. M. Skotheim, J. Dumais, and L. Mahadevan. How the venus flytrap snaps. *Nature*, 433(7024):421–425, 2005.

Y. Forterre, P. Marmottant, C. Quilliet, and X. Noblin. Physics of rapid movements in plants. *Europhysics News*, 47(1):27–30, 2016.

O. Gaycken. The secret life of plants: Visualizing vegetative movement, 1880–1903. *Early Popular Visual Culture*, 10(1):51–69, 2012.

A. Goriely. *The mathematics and mechanics of biological growth*, volume 45. Springer, 2017.

H. Gradmann. *Die funfphasenbewegung der ranken.* 1922.

P. Green, R. Erickson, and J. Buggy. Metabolic and physical control of cell elongation rate: in vivo studies in nitella. *Plant Physiology*, 47(3):423–430, 1971.

K. T. Haas, R. Wightman, E. M. Meyerowitz, and A. Peaucelle. Pectin homogalacturonan nanofilament expansion drives morphogenesis in plant epidermal cells. *Science*, 367(6481):1003–1007, 2020.

H. Höfte, A. Peaucelle, and S. Braybrook. Cell wall mechanics and growth control in plants: the role of pectins revisited. *Frontiers in plant science*, 3:121, 2012.

D. Israelsson and A. Johnsson. A theory for circumnutations in helianthus annuus. *Physiologia Plantarum*, 20(4):957–976, 1967.

K. Jensen and Y. Forterre. *Soft matter in plants: from biophysics to biomimetics*, volume 15. Royal Society of Chemistry, 2022.

A. Johnsson. Circumnutations: results from recent experiments on earth and in space. *Planta*, 203(1):S147–S158, 1997.

A. Johnsson and D. Israelsson. Application of a theory for circumnutations to geotropic movements. *Physiologia Plantarum*, 21(2):282–291, 1968.

A. Johnsson, C. Jansen, W. Engelmann, and J. Schuster. Circumnutations without gravity: a two-oscillator model. *J Gravit Physiol*, 6(1):P9–12, 1999.

B. M. Jordan and J. Dumais. Biomechanics of plant cell growth. *eLS*, 2010.

D. Kierzkowski, N. Nakayama, A.-L. Routier-Kierzkowska, A. Weber, E. Bayer, M. Schorderet, D. Reinhardt, C. Kuhlemeier, and R. S. Smith. Elastic domains regulate growth and organogenesis in the plant shoot apical meristem. *Science*, 335 (6072):1096–1099, 2012.

T. Kincaid. The complex representation of signals. *TIS R67# MH5, General Electric Co*, 1966.

L. Kozlova, A. Petrova, B. Ananchenko, and T. Gorshkova. Assessment of primary cell wall nanomechanical properties in internal cells of non-fixed maize roots. *Plants*, 8 (6):172, 2019.

J. H. Kroeger, R. Zerzour, and A. Geitmann. Regulator or driving force? the role of turgor pressure in oscillatory plant cell growth. *PloS one*, 6(4):e18549, 2011.

D. Kwiatkowska. Flower primordium formation at the arabidopsis shoot apex: quantitative analysis of surface geometry and growth. *Journal of Experimental Botany*, 57 (3):571–580, 2006.

D. Kwiatkowska and J. Dumais. Growth and morphogenesis at the vegetative shoot apex of anagallis arvensis l. *Journal of Experimental Botany*, 54(387):1585–1595, 2003.

D. Kwiatkowska and A.-L. Routier-Kierzkowska. Morphogenesis at the inflorescence shoot apex of anagallis arvensis: surface geometry and growth in comparison with the vegetative shoot. *Journal of experimental botany*, 60(12):3407–3418, 2009.

H. Lambers and H. Poorter. Inherent variation in growth rate between higher plants: a search for physiological causes and ecological consequences. In *Advances in ecological research*, volume 23, pages 187–261. Elsevier, 1992.

J. A. Lockhart. An analysis of irreversible plant cell elongation. *Journal of theoretical biology*, 8(2):264–275, 1965.

Y. Long, I. Cheddadi, G. Mosca, V. Mirabet, M. Dumond, A. Kiss, J. Traas, C. Godin, and A. Boudaoud. Cellular heterogeneity in pressure and growth emerges from tissue topology and geometry. *Current Biology*, 2020.

F. Micheli. Pectin methylesterases: cell wall enzymes with important roles in plant physiology. *Trends in plant science*, 6(9):414–419, 2001.

F. Migliaccio, P. Tassone, and A. Fortunati. Circumnutation as an autonomous root movement in plants. *American journal of botany*, 100(1):4–13, 2013.

P. Milani, M. Gholamirad, J. Traas, A. Arnéodo, A. Boudaoud, F. Argoul, and O. Hamant. In vivo analysis of local wall stiffness at the shoot apical meristem in arabidopsis using atomic force microscopy. *The Plant Journal*, 67(6):1116–1123, 2011.

D. E. Moulton, T. Lessinnes, and A. Goriely. Morphoelastic rods iii: Differential growth and curvature generation in elastic filaments. *Journal of the Mechanics and Physics of Solids*, 142:104022, 2020a.

D. E. Moulton, H. Oliveri, and A. Goriely. Multiscale integration of environmental stimuli in plant tropism produces complex behaviors. *Proceedings of the National Academy of Sciences*, 117(51):32226–32237, 2020b.

S. Mugnai, E. Azzarello, E. Masi, C. Pandolfi, and S. Mancuso. Nutation in plants. In *Rhythms in plants*, pages 19–34. Springer, 2015.

X. Noblin, N. Rojas, J. Westbrook, C. Llorens, M. Argentina, and J. Dumais. The fern sporangium: a unique catapult. *Science*, 335(6074):1322–1322, 2012.

H. Oliveri and I. Cheddadi. Hydromechanical field theory of plant morphogenesis. *Journal of the Mechanics and Physics of Solids*, 196:106035, 2025. ISSN 0022-5096. doi: https://doi.org/10.1016/j.jmps.2025.106035. URL https://www.sciencedirect.com/science/article/pii/S0022509625000110.

V. Orbović and K. L. Poff. Interaction of light and gravitropism with nutation of hypocotyls of arabidopsis thaliana seedlings. *Plant growth regulation*, 23(3):141–146, 1997.

J. K. Ortega. Augmented growth equation for cell wall expansion. *Plant physiology*, 79 (1):318–320, 1985.

R. Palin and A. Geitmann. The role of pectin in plant morphogenesis. *Biosystems*, 109 (3):397–402, 2012.

A. Peaucelle, S. A. Braybrook, L. Le Guillou, E. Bron, C. Kuhlemeier, and H. Höfte. Pectin-induced changes in cell wall mechanics underlie organ initiation in arabidopsis. *Current biology*, 21(20):1720–1726, 2011.

W. S. Peters and A. D. Tomos. The mechanic state of “inner tissue” in the growing zone of sunflower hypocotyls and the regulation of its growth rate following excision. *Plant Physiology*, 123(2):605–612, 2000.

H. Poorter and C. Remkes. Leaf area ratio and net assimilation rate of 24 wild species differing in relative growth rate. *Oecologia*, 83(4):553–559, 1990.

T. E. Proseus, J. K. Ortega, and J. S. Boyer. Separating growth from elastic deformation during cell enlargement. *Plant physiology*, 119(2):775–784, 1999.

M. Quiros, M.-B. Bogeat-Triboulot, E. Couturier, and E. Kolb. Plant root growth against a mechanical obstacle: the early growth response of a maize root facing an axial resistance is consistent with the lockhart model. *Journal of the Royal Society Interface*, 19(193):20220266, 2022.

M. Rivière. *Shape, rhythms and growth heterogeneities of a leaf: unfurling and nutation of Averrhoa carambola: Forme, rythmes et hétérogénéités de croissance d'une feuille: déroulement et nutation chez Averrhoa carambola´*. PhD thesis, Sorbonne Paris Cité, 2017.

M. Rivière, J. Derr, and S. Douady. Motions of leaves and stems, from growth to potential use. *Physical biology*, 14(5):051001, 2017.

M. Rivière, Y. Corre, A. Peaucelle, J. Derr, and S. Douady. The hook shape of growing leaves results from an active regulatory process. *Journal of Experimental Botany*, 71(20):6408–6417, 2020.

R. Sachse, A. Westermeier, M. Mylo, J. Nadasdi, M. Bischoff, T. Speck, and S. Poppinga. Snapping mechanics of the venus flytrap (dionaea muscipula). *Proceedings of the National Academy of Sciences*, 117(27):16035–16042, 2020.

W. K. Silk. Quantitative descriptions of development. *Annual Review of Plant Physiology*, 35(1):479–518, 1984.

W. K. Silk. Steady form from changing cells. *International Journal of Plant Sciences*, 153(3, Part 2):S49–S58, 1992.

W. K. Silk, E. M. Lord, and K. J. Eckard. Growth patterns inferred from anatomical records: empirical tests using longisections of roots of zea mays l. *Plant Physiology*, 90(2):708–713, 1989.

M. Stolarz. Circumnutation as a visible plant action and reaction: physiological, cellular and molecular basis for circumnutations. *Plant signaling & behavior*, 4(5):380–387, 2009.

M. Stolarz, E. Krol, H. Dziubinska, and T. Zawadzki. Complex relationship between growth and circumnutations in helianthus annuus stem. *Plant signaling & behavior*, 3(6):376–380, 2008.

S. Timoshenko. Analysis of bi-metal thermostats. *Journal of the Optical Society of America*, 11(3):233–255, 1925.

A. D. Tomos, M. Malone, and J. Pritchard. The biophysics of differential growth. *Environmental and experimental botany*, 29(1):7–23, 1989.

A. Walter, H. Spies, S. Terjung, R. Kusters, N. Kirchgessner, and U. Schurr. Spatio-¨ temporal dynamics of expansion growth in roots: automatic quantification of diurnal course and temperature response by digital image sequence processing. *Journal of experimental botany*, 53(369):689–698, 2002.

C. Webster. The recognition of plant sensitivity by english botanists in the seventeeth century. *Isis*, 57(1):5–23, 1966.

R. Zerzour, J. Kroeger, and A. Geitmann. Polar growth in pollen tubes is associated with spatially confined dynamic changes in cell mechanical properties. *Developmental biology*, 334(2):437–446, 2009.

G. L. Zhu and J. S. Boyer. Enlargement in chara studied with a turgor clamp: growth rate is not determined by turgor. *Plant Physiology*, 100(4):2071–2080, 1992.

Graphical_Abstract